A comparison of the innate flexibilities of six chains in F_1-ATPase with identical secondary and tertiary folds; 3 active enzymes and 3 structural proteins

Monique M. Tirion[1, a)]

Physics Department, Clarkson University, Potsdam, New York 13699-5820, USA

arXiv:1608.02976v2 [q-bio.BM] 5 Nov 2016

The α and β subunits comprising the hexameric assembly of F1-ATPase share a high degree of structural identity, though low primary identity. Each subunit binds nucleotide in similar pockets, yet only β subunits are catalytically active. Why? We re-examine their internal symmetry axes and observe interesting differences. Dividing each chain into an N-terminal head region, a C-terminal foot region, and a central torso, we observe (1) that while the foot and head regions in all chains obtain high and similar mobility, the torsos obtain different mobility profiles, with the β subunits exhibiting a higher motility compared to the α subunits, a trend supported by the crystallographic B-factors. The β subunits have greater torso mobility by having fewer distributed, nonlocal packing interactions providing a spacious and soft connectivity, and offsetting the resultant softness with local stiffness elements, including an additional β sheet. (2) A loop near the nucleotide binding-domain of the β subunits, absent in the α subunits, swings to create a large variation in the occlusion of the nucleotide binding region. (3) A combination of the softest three eigenmodes significantly reduces the RMSD between the open and closed conformations of the β subnits. (4) Comparisons of computed and observed crystallographic B-factors suggest a suppression of a particular symmetry axis in an α subunit. (5) Unexpectedly, the soft intra-monomer oscillations pertain to distortions that do not create inter-monomer steric clashes in the assembly, suggesting that structural optimization of the assembly evolved at all levels of complexity.

[a)]Electronic mail: mmtirion@clarkson.edu

I. INTRODUCTION

A. Overview of hexameric F_1-ATPase

ATP synthases exploit ion gradients generated during electron transport reactions at cell interfaces to phosphorylate ADP and replenish the cell's supply of ATP. Mild salt treatments dissociate ATP synthases into two fractions: a membrane-embedded F_o portion and a soluble, hydrophilic F_1 portion (for reviews, see[1–3]). In the intact enzyme, the F_o portion links an ionic gradient to a mechanical rotation, while the F_1 portion channels the rotary motion to the synthesis reaction. The dissociated F_1 portion lacks the capacity to generate ATP, however it does function as an ATPase, hydrolyzing ATP in the presence of ATP, ADP and phosphate, P_i. The isolated F_1 complex consists of five different protein chains with stoichiometries of $\alpha_3\beta_3\gamma_1\delta_1\epsilon_1$ and mass ratios 55, 51, 31, 15 and 6 kD. F_1 fractions obtained from bacteria, fungi, animals and plants have been crystallized and their atomic positions resolved and reveal this enzyme complex to possess a highly conserved structure[4,5].

As illustrated in Figure 1, in F_1-ATPase the three α subunits (SUA) and three β subunits (SUB) alternate as the segments of an orange to create a cap-like structure with an outer diameter of around 100Å and a central channel about 20Å across. This central channel, marking the axis of pseudosymmetry, contains a pair of coiled-coil α helices formed by the N and C terminal domains of the γ subunit. The remainder of the γ chain as well as the smaller δ and ϵ chains form a globular arrangement attached to the central α helices like the head of a golf club to its shaft.

The X-ray structures show the α and β chains to possess nearly identical three-dimensional conformations with all-atom root mean square difference (RMSD) superpositions between 2.2 and 2.6Å, but with primary sequence identity and similarity of 25% and 43%[6]. Adenosyl nucleotides can bind to each SUA and SUB in binding pockets located at their interfaces. However, only SUB is catalytically active: ATP bound to SUA is neither hydrolyzed nor exchanged with solvent medium[7–9]. Catalysis at the three β subunits occurs not with use of high energy intermediates, but in a cooperative, cyclic fashion termed the binding change mechanism[10]. Studying heavy oxygen exchange rates during ATP synthase catalysis in the presence and absence of a proton gradient, Boyer realized that the pmf at F_o is energetically coupled with product release at F_1 rather than chemical bond-formation. Once bound to a

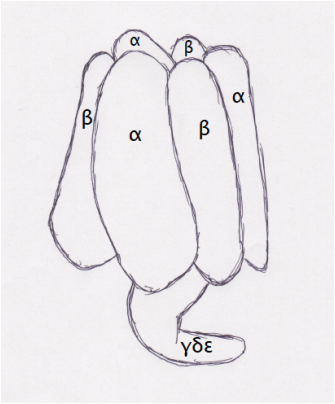

FIG. 1. Schematic of the F_1-ATPase fragment of ATP synthase. Composed of alternating α and β subunits, the central axis of pseudosymmetry obtains an α-helical coiled coil from the N and C terminal domains of the γ subunit, while the remainder of that subunit plus the δ and ϵ chains protrude from the central channel below the foot domains. The hexameric cap has a diameter of around 100Å.

catalytic site, in other words, ADP and P_i spontaneously interconvert to ATP without external energy and have an equilibrium constant close to 1. According to the binding change mechanism, each β subunit sequentially binds ADP and P_i, then undergoes a conformational transition and makes ATP, and finally changes conformation again with release of product. The three subunits function in concert, with each subunit cycling through the same states consecutively, so that the system"hangs" if one subunit is prevented from transitioning, by for example, removal of product from solvent medium. Experiments suggest that the rotary, cyclic behavior of the hexamer persists during hydrolysis in the absence of the γ chain, though with lower precision and rate constants[11–13].

Our current analyses will focus on the elements comprising this minimal functional unit, the α and β chains. In particular, we examine the question: why do β subunits readily hydrolyze ATP and exchange the HOH generated with medium water, while the α subunits neither hydrolyze nor exchange ATP with solvent nucleotides? Xu and coworkers[1] point

out that while the nucleotide-binding sites in α and β subunits are closely conserved, one carboxylate, of residue β-Glu 188 is replaced by α-Gln 208, eliminating a likely catalytic base in the α subunits. Furthermore, Xu points out that the α subunit's "inability to transition between different catalytic conformations ... as evidenced by the absence of open conformation" in crystalline structures, severely dampens their catalytic activity. In this work we closely examine the extent and reason for the "inablity" of α subunits to cycle through the conformations adopted by the β subunits. Superficially, one might expect two proteins with such similar fold and architecture to exhibit similar flexibility characteristics. In particular, then, the internal symmetry axes of these different protein chains should be nearly identical. Are they? We compute and examine each proteins' slowest eigenmodes via PDB-NMA. We observe interesting similarities and differences that may help further explain the different catalytic propensities of these two subunits.

B. Overview of PDB-NMA

Just as rigid structures obtain 3 rotational principal symmetry axes determined by diagonalization of their inertia matrix, nonrigid objects obtain internal symmetry axes derived from diagonalization of their Hessian matrix[14]. An object has as many internal symmetry axes or eigenvectors as it has internal degrees of freedom, with each eigenvector a specific linear combinatiton of those internal degrees of freedom. The Hessian matrix of an object describes the distribution, not of masses, but of forces about a position of stability as its internal degrees of freedom are varied. Rigid principal axes pertain to spatial symmetries where the mass distributions about each of 3 special, orthogonal axes are balanced and the angular velocity and momentum vectors aligned. Nonrigid, internal axes pertain to temporal symmetries: each axis pertains to a balanced, internal oscillation of the object with one particular frequency and energy. These axes are orthogonal and hence also known as normal modes: excitation of one mode cannot excite another mode, though in practice anharmonicities introduce off-diagonal elements that decohere motion. As the normal modes describe oscillations innate or intrinsic to the system, the modes are often referred to as eigenmodes and they form a complete, orthonormal coordinate system.

The set of frequencies obtained by diagonalization of the object's Hessian, called the eigenspectrum, has a characteristic distribution for proteins, different from other solids[15–17].

The highest frequencies arise from rapid vibrations of the stiffest elements while the slowest frequency is a function of the mass and shape of the molecule, and is roughly 0.1 THz for a 50kDa protein (spectroscopists attempt to probe such motions by delivering photons with identical frequencies and often report this in terms of the corresponding photon wavenumber of 3 cm^{-1}.)

In addition to the eigenfrequencies, the diagonalization of the Hessian matrix provides the set of vectors or eigenmodes that describe the shape of the motion associated with each eigenfrequency. As folded, globular proteins obtain high packing densities and heat capacities comparible to solid crystalline objects[18], it is interesting to ascertain how correlated motions extending over the entire molecule are enabled. Snapshots of single conformations cannot convey this information and one cannot anticipate how a particular molecule "solves" the problem of enabling large-scale motions where thousands (internal) degrees of freedom cooperatively deform tens of thousands of nonbonded interactions to achieve correlated motions across the entire molecule or "full body motion," FBM.

The innate dofs associated with equilibrium oscillations describe motilities of interest: energy imparted to an object at rest will be dissipated by these internal degrees of freedom. Unlike spectroscopists who deliver very precise energy pulses that may match particular molecular frequencies[19], thermal baths activate folded protein's many modes equally. No particular dof dissipates the thermal energy, instead the heat energy is distributed amongst all the internal symmetry axes. The high frequency modes dissipate the kT thermal units in high frequency, low amplitude oscillations while the slowest modes dissipate kT energy units in low frequency, larger amplitude oscillations. There is a longstanding assumption that nature exploits the long-correlation length "slow" motions intrinsic in folded proteins to achieve functionality[20].

C. Range of validity

Normal modes provide another "quality" or signature of an object much as do mass or charge distributions, heat capacity, reflectivity, shape, etc, independent of the basis vectors chosen to describe that object's internal degrees of freedom[21]. For this reason, the modes computed using all-atom Cartesian degrees of freedom or heavy-atom dihedral degrees of freedom or reduced coordinates such as a single point per residue, match for sufficiently slow

frequency modes.

All-atom analyses on PDB entries using detailed force fields such as Gromos or Charmm are accurate but handicapped by the fact that PDB entries are not at equilibrium according to these parameterizations[22]. Therefore, prior to diagonalization of the Hessian, an initial structure-distorting energy minimization *must* be performed. Minimization of objects with thousands of degrees of freedom and tens or hundreds of thousands of energy terms is not an exact, analytic process, and no single, unique minimized structure exists, even under a particular force field. Furthermore, the tens of thousands of nonbonded terms have exquisitely sensitive dependencies on their distances of separation that result in the rapid accumulation of round-off errors for the floating point representations of the energy per conformation. In practice this means that a minimal energy conformation can not be discerned using double precision computations for proteins larger than around 150 residues. The resulting negative eigenvalues describe unstable motions that are typically ignored and that complicate the analysis of the remaining positive, stable eigenmodes. One can avoid these limitations by accepting each PDB entry as representing a stable conformation, a not unreasonable assumption given that typically 10^{17} molecules align identically to provide high resolution X-ray diffraction data[23]. This assumption, that the PDB entry represents a stable, long-lived conformation, permits design of simplified, Hookean force fields to describe equilibrium oscillations[24]. While initial parameterizations of such Hookean force fields were necessarily maximally simple, current formulations carefully parameterize every bonded and nonbonded term in accordance to a "parent" potential such as ENCAD or CHARMM[25,26]. The resultant eigenspectra and eigenmodes reproduce those obtained using the parent potentials *when done on the same, energy minimized coordinates.* Consequently, use of these Hookean force fields permits comparison of the eigenspectra and eigenmodes of two closely similar structures, such as the A and B populations within a single protein crystal[27] or the α and β chains of F_1-ATPase.

Our current analyses are based on a reduced heavy-atom representation, inclusive all atoms in the PDB entries, as provided by the force field developed by Michael Levitt, termed L79[28], the precursor to ENCAD[29]. In L79, the energy of each pair of (ϕ, ψ) main-chain torsions is modeled as a sum of Gaussian-like potentials, a functional that reproduces Ramachandran maps and compensates for the exclusion of nonbonded interactions between atoms separated by three bonds; while the energy associated with sidechain torsions is mod-

eled by a harmonic functional. Nonbonded, dispersive and repulsive forces between all atoms more than three bond lengths and less than some cutoff distance apart are modeled by a Lennard-Jones 6-12 potential. L79 includes only polar hydrogens, with hydrogens bonded to carbons combined into united forms.

This early formulation of an intra-molecular force field works well for modeling the motility of large, isolated globular proteins. To better characterize surface forces involved in ligand binding, inter-molecular interactions and water, especially to reaction pathways, more sophisticated potentials evolved. Our current interest pertains to analyses of entire molecule, full-body motions, FBM, that examines the concurrent activation of thousands of internal dofs that cooperatively deform tens of thousands of NBI. While a Hookean force field has a seemingly trivial complexity and range of validity (namely, at a point of equilibrium), the space where several thousand constrained degrees of freedom (dihedral angles) exist in a force field consisting of tens of thousands of nonbonded pairwise interactions is rich and surprising. Achievement of self-consistency in this vast space, both in terms of the mathematical formulations as well as in machine encoding, is essential to link effects and causes. The addition of complexity to this formulation, by inclusion of all hydrogen atoms and crystal and solvent waters for example, is desirable, but their contributions to the FBM can only be discerned and ultimately understood in contrast to the formulation lacking these elements. For this reason, we characterize the equilibrium motility spectra of PDB entries primarily using the simpler L79 potential, and only briefly consider the contributions within the current formulation of ligands, including nucleotides, cations and crystal HOH.

Normal mode studies of the F_1-ATPase structure with the PDB designation[30] 1BMF[31] have been published by Cui and coworkers[32] as well as by Zheng[33]. The latter uses a coarse-grained elastic network model to study the coupling of cyclic conformational transitions, as modeled by intramonomer hinges and intermonomer rigidy body motions, and γ subunit rotations to ATP binding and product release. The former, earlier, study used all heavy atoms as well as polar hydrogen atoms, ligands and crystal waters in a classical (non-Hookean) force field in order to characterize the structural plasticity of the isolated α, β and γ subunits, as well as the $\alpha_3\beta_3\gamma$ assembly. These analyses required initial energy minimizations that distorted the crystal coordinates by RMSD values of around 1Å. Cui and coworkers published the root mean square fluctations or RMSF per C_α of the intramonomer vibrations of the α, β and γ subunits, as well as for the complex. Each β subunit,

they concluded "has the functionally relevant flexibility built into its structure". Our results reproduce the RMSF plots for the α and β subunits, and indicate that the FBM patterns associated with the energy minimized 1BMF structures are largely shared by those of the current PDB entry. Our analyses add to the insights provided by the earlier studies by probing the nature and cause of the variable flexibility of the α and β subunits. We continue efforts to develop a lexicon to describe nonlocal FBM where the motility of any particular loop is causally linked with the motility of all parts of the peptide chain. Highly mobile loops, it is seen, are not mobile in isolation: regions may be stiff locally and yet obtain high temperature factors. We examine the correlations of computed and observed temperature factors and note an interesting signature suggesting the absence of one particular mode of vibration in an α subunit.

D. Homunculus

To characterize nonlocal FBM, it will be helpful to adopt and extend a descriptive vocabulary. Figure 2 presents a schematic diagram of one subunit to provide a contextual lexicon for the regions relevant to FBM. The N terminal "head" domain, a six-stranded β barrel extending from the N terminus to residue β Asp 77 and α Ile 94, is *superior* to the "torso," the nucleotide-binding domain consisting of a seven-stranded parallel β sheet and associated α helices. The C-terminal "foot" domain, a bundle of 6 (β subunit) or 7 (α subunit) α helices is *inferior* to the torso in this representation. Each subunit forms two interfaces within the hexamer: with the central, rotor axis situated *internal* to the subunit, a *ventral* surface involving the subunit's nucleotide-binding domain, as well as a *dorsal* surface that abuts the neighboring subunit's nucleotide-binding region, are indicated in Figure 2.

The torso's central β sheet extends diagonally from the inferior dorsal region to the superior ventral region. The C-terminal, arrowed ends of the β strands orient towards the internal surface of the hexamer, at a lower radial distance from the central axis than the N terminal ends of the β strands which orient towards the *external* surface of the hexamer. The *anterior* surface of the torso's β sheet faces the head region and obtains 4 α helices and associated loops. The *posterior* surface of the β sheet faces the foot and obtains two α helices (B and C) as well as the P-loop that binds nucleotide and cation.

The head domain links to the torso domain via a short "neck". A long linker "arm"

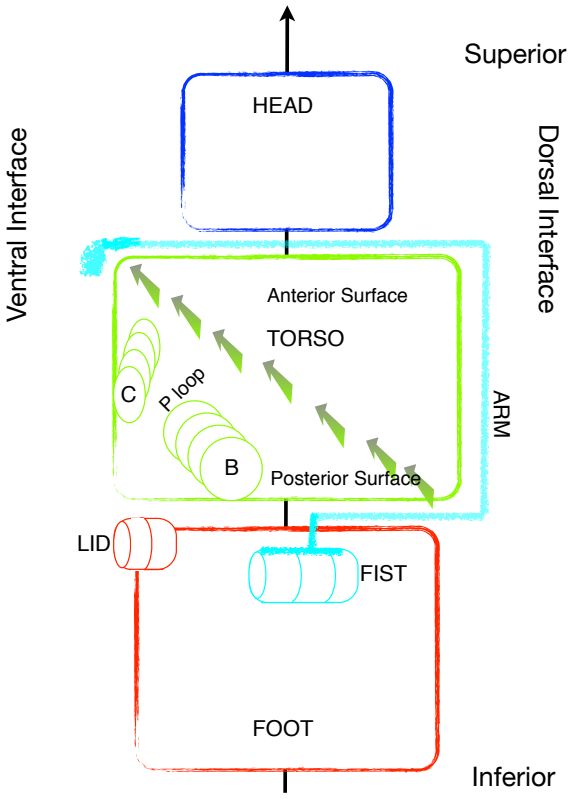

FIG. 2. Schematic representation of subunit. Each subunit consists of three domains, a head, torso and foot. Viewed from the external surface, the axis of pseudosymmetry as indicated by the solid arrow, is behind the subunit in this representation. Each subunit interacts with two neighbors in the hexamer: at the ventral surface and at the dorsal surface. The torso is divided into an anterior and a posterior surface region by a seven stranded parallel β sheet that extends from the inferior dorsal region to the superior ventral region. The posterior surface of the β sheet consists of the nucleotide binding region including the P-loop and helices B and C. A shoulder region at the interface of the head and torso near the ventral surface extends as an arm along the anterior surface to connect to the foot domain as a short α helix, the fist.

extending from residues β Asp 103 - Ile 137 and α Asp 116 - Ile 150 drapes along the outer surface of the torso from the head region to the foot region where it connects to a firmly embedded short α helix, the "fist," at residues β 138-143 and α 151-155. A "shoulder"

region extending from the neck to the arm is situated superior to the torso at the ventral surface. The superior, ventral region of the foot domain contributes either a highly mobile "lid" (β Pro 417 - Pro 433) or a shorter "strut" (α Gln 430 - Glu 440) that serve to either enhance or dampen oscillatory motions at the nucleotide-binding cleft.

II. RESULTS

A. PDB coordinates

We use the α and β chains from coordinate file 2JDI[34]. For this structure, mitochondrial F_1-ATPase from bovine heart tissue was crystallized in the absence of preservatives and inhibitors and in the presence of ADP and a non-hydrolyzable ATP analog AMP-PNP (abbreviated as ANP) and solved to 1.9Å resolution. The 3 α subunits, chains A, B and C, as well as two β chains, D and F, each contain ANP and cation in their nucleotide-binding pockets while the remaining β subunit, chain E, contains no nucleotide nor cation. Each chain folds to fit inside a wedge about 85Å along the central axis, 50Å in the radial direction, and 55Å along the radial arc. By convention, each β subunit is paired with the neighboring α subunit that abuts and contributes to that β subunit's catalytic site: E with A, F with B and D with C.

In 2JDI the three α chains adopt almost identical conformations. Their all-atom superpositions result in RMSD values of 0.6-0.7 Å, with minor mismatches in the alignment of either their head or foot regions. The β chains D and F, both containing ANP and Mg, obtain an RMSD of 0.6Å. Chain E, lacking nucleotide and cation, differs from the other two β chains by 3.8 Å. The E chain's head and foot regions have swung to a higher radial distance from the central axis, creating a more open or extended conformation. Superposing the individual head, torso and foot domains of chains E and F results in RMSD values of 0.2Å, 1.3Å and 0.5Å, indicating that the nearly 4Å shift between these two chains is created to a large extent by rigid body rotations of these three domains.

The α chains extend from residues 24-510 and the β chains from 9-474 (we maintain the PDB numbering convention that labels the N terminal βAla residue as 1, not -4). Chain C, as an example, obtains 3715 atomic coordinates, whose 11145 internal, Cartesian degrees of freedom divide among 3766 bond lengths, 4768 bond angles, 2605 dihedral angles and 6

rigid body degrees of freedom. We include only the "soft" dihedrals, including 469 ϕ, 487 ψ and 873 χ angles, to study thermally induced equilibrium vibrations, reducing the available degrees of freedom from 11139 to 1829 while maintaining all bond lengths and angles to PDB values. In addition to the energies associated with these dofs, chain C obtains 22160 non bonded interactions (NBI) between all atom pairs further apart than 3 bond lengths and less than a cutoff distance defined by the inflection point of their van der Waal curves. The average NBI per atom is 5.3 and includes roughly the first shell of neighbors. The total NBI divide between 9461 main chain-main chain interactions, 9222 main chain-side chain interactions, and 3477 side chain-side chain interactions. While we report on this distribution of dihedral angles and NBI, one might examine the effects of eliminating particular groups of NBI or soft dihedrals on the motility spectra, to assess, for example, the effects of mutations on motility[27]. (In the isolated protein, the two different orientations of surface SC Arg 373 from chain A do not affect the slow modes here described.)

B. Normal Modes

Normal modes were computed using ATMAN[26]. Thermal activations of modes were computed at 180K, the temperature observed to divide harmonic from anharmonic motion in folded proteins[35] and close to the crystal temperature of 100K. RMSF values per mode decrease rapidly with mode number, with the first three modes contributing 64% to the total, therefore our focus remains on these three softest, slowest modes[36]. Most analyses were carried out on chains C and F to study the distinct signatures of SUA and SUB. Residue to residue comparisons between chains belonging to subsets α and β used the Needleman & Wunsch sequence alignment algorithm available from the Protein Data Bank[6]. Results were checked for consistency using chains D and A. Chains B and E both miss an 8 residue sequence in the foot (α 402-409, β 388-395) in a region with high experimental temperature factors (over 60Å^2 when the mean B-factor for chains A-F is 16Å^2). To test for consistency with chains B and E, the missing 8 residues were built-in by rigid body alignment of the missing region from a neighboring subunit.

In all, the computed modes describe the same motions, both among chains A, B and C as well as among chains D, E and F. For example, Figure 3 shows the RMSF per C_α due to the combined effects of modes 1, 2 and 3 for chains D, E and F, the three β subunits.

The computed motility profiles for these 3 chains superpose almost perfectly, with chain E presenting with slightly different RMSF amplitudes in the region that includes helix C (residues β190 - 215) as well as a loop on the anterior side of the torso's β sheet (residues β317-321). These plots closely match the equivalent RMSF per C_α plot for the unliganded β subunit, Figure 10a, of Cui and coworkers[32], with the mismatch in relative amplitudes due to our use of 180K for the activation temperature and our use of a small subset of all modes.

While the similarity of the slow modes amongst the α chains is not surprising due to the close structural similarity between these chains, the match of the slow modes amongst the different β chains is reassuring. The E chain adopts a conformation distinct from chains D and F, and the similarity of the three β chain mobility profiles provides a strong indication of the intrinsic character of these innate dofs. One might therefore expect eigenmodes to contribute to the interconversion of these different conformations.

As discussed in the Introduction, the current analyses pertain primarily to the computed eigenspectra of the α and β subunits in absence of bound ligands. The β subunits transition between open and closed conformations as reactants enter and products leave the catalytic site. Furthermore, 2JDI reports 351 $\pm$ 16 crystal water molecules for the three α subunits, and 351 $\pm$ 85 crystal waters for the three β subunits, indicating a large variation in the numbers of crystal waters accompanying the structural transitions. To assess the extent to which ligands affect the expression of the slowest modes, we computed the eigenspectra and eigenvectors of the protein plus nucleotide and cation; protein plus tight bound waters; and protein plus nucleotide, cation and tight bound waters. A water molecule was considered tightly bound if it obtained atleast 5 NBI with protein atoms. We find that the presence of nucleotide and cation slightly shifts the frequencies of the slowest modes, making them stiffer and resulting in slightly smaller amplitudes of oscilllation at any given temperature. The presence of tightly bound waters slightly alters the slow eigenvector shapes, tending to enhance the propensity seen in the β subunits to open and close the catalytic site. As the effects of ligands on the slow modes as modeled by L79 do not result in significant differences, we here focus our research on the isolated protein chains.

The use of unliganded protein chains is supported by earlier analyses of the liganded and unliganded motility profiles of β subunits[32,37,38] which show RMSF per C_α shifts only in the magnitudes of certain peaks. Such shifts imply changes in the amplitudes of motions, not

changes in the character of the motion. For example, Hahn-Herrera and coworkers recently published results of MD simulations of isolated α and β chains of PDB entry 2JDI[37]. In addition to the protonated PDB coordinates, ATP and cation, his group included 40,338 water molecules in the system. After 10 ns of equilibration, the system underwent 100 ns of unbiased MD simulation. The resultant RMSF values of the C_α atoms of chain F (liganded β subunit) is shown as the orange line in Figure 4 (data kindly provided by Prof. Garcia-Hernandez). Current NMA predictions due to the slowest 50 modes for the same chain, unliganded and up-scaled by a factor of 2.6, are superposed with the black line. Harmonic oscillations at 300K rather than the 180K used here, increase the amplitudes of oscillation by a factor of $\sqrt{300/180}$ or 1.3. Furthermore, anharmonic contributions in MD are thought to double predicted displacements compared to harmonic NMA[39] and may explain this scaling factor. The motility patterns for the head, shoulder, arm and posterior surface of the torso domain match closely. The peaks associated with those regions closest to the central γ axis, such as the DELSEED loop, are also matched, though with slight mismatches in their magnitudes. By and large, therefore, the long-term, 100 ns, motility profile of a solvated protein chain derived from a detailed and accurate force field matches that predicted by PDB-NMA. This match provides a strong indication that long term motility is the result of correlated motions and not the result of separate regions moving independently. The NMA profile, produced by the superposition of all the modes of oscillation, may be separated into and studied as individual modes in an effort to characterize and apprehend the source of these long-term motility profiles.

C. The first three modes

The slowest three modes of SUA and SUB obtain similar profiles for the FBMs involving relative displacements of the head, torso and foot regions. While computed using dihedral angles, the slowest three modes are also perpendicular in Cartesian space, with oscillations of mode 1 about an axis aligned along a radial direction; of mode 2 about a radial arc and for mode 3 about a direction parallel to the central, γ axis. While the oscillations described by each mode appear largely similar between SUA and SUB, their effects on the posterior side of the β sheet, and in particular on the cleft that ends at the Walker A motif or P-loop (GxxxxGKT, residues α 169-177 and β 156-163) that coordinates the β phosphate of the

nucleotide, is very distinct. In SUB this cleft extends approximately 20 Å along a radial direction to the external surface with its base formed by helix B extending from the P-loop (Figure 5A). The top of the cleft is formed by helix C and the bottom by the lid, with βPhe 424 aligned with the ribose ring. This cleft in SUB displays pronounced opening and closing motions for modes 1 and 2 and a relative, grinding motion in mode 3, motions completely absent in the α subunits. The mobile lid is not present in SUA where the strut blocks relative motion across the crevasse, with foot residue αTyr 433 forming extensive steric interactions with α Arg 219 from the top of the cleft (Figure 5B).

The slowest modes of SUA and SUB (Figures 6A and 6B), with frequencies of α 2.6 cm^{-1} and β 2.7 cm^{-1}, pertain to a sidewise rolling, with the head and foot regions rocking towards each other along a radial axis closely aligned with the P-loop helix (B). The arm in SUB seems to function as a caliper, with the C_αs of shoulder residues Asp 103 and fist Gly 136 separating 33.2 $\pm$ 1.2Å. This results, on the other side of the torso's β sheet, in a sizable fluctuation of nearly 3Å between the top of the cleft and the mobile lid, in an up-and-down chewing type motion. In SUA, the rolling of the head towards and away from the foot along a radial axis is again observed. However, the arm in SUA does not function as a caliper, and the equivalent C_α atoms at residues Asp 116 and Gly 149 remain at a nearly steady 28.5$\pm$0.2Å separation during thermal activation. As a result, the cleft and access to the cleft leading to the P-loop is not distorted.

Modes 2 (Figures 6C and 6D), both with frequency of 3.1 cm^{-1}, pertain to a flexing toward the central axis, with a short stationary α helix oriented along a radial arc marking the axis about which the top and bottom portions of the chain oscillate. This short helix is the fist that interconnects the head and foot regions, moving in tight synchrony with the foot domain due to extensive packing interactions, including SUB residues Lys 138, Val 139 and Leu 142 and Leu 143. The NZ of Lys 138, for example, maintains fixed distances of separation with the main chain carbonyl oxygens of Arg 142, Phe 457, Gly 461, Phe 413 and Val 460 during thermal activation. The effect, as seen in Figure 6C, is startling: the fist residues β 138-143 (indicated by the short, left-most vertical arrow), obtain low RMSF values along with those nearby regions of the foot indicated by the remaining vertical arrows. Several of the α helices in the foot radiate away from the fist region, with those regions of the helices near the fist nearly immobile while the remainder of these helices obtain significant RMSF values. For example, the C terminal region of helix β399-414 and the N terminal region

of helix β434-448 obtain small RMSF values (right most arrows), while their connecting loop forms the mobile lid motif. As a result, the head and foot regions simultaneously rock towards and away from the central γ axis, with the nucleotide binding cleft experiencing a more pronounced opening nearer the P-loop rather than near the outer edge as in mode 1. The second mode, as will be seen, contributes the largest amplitude when the slow modes are used as $dofs$ to transform the coordinates of the D and F chain to the E chain.

Modes 3 (Figures 6E and 6F), with computed frequencies of α 3.8 cm^{-1} and β 3.6 cm^{-1}, pertain to a twisting motion of the head and foot regions about an axis roughly parallel to the central γ axis. This motion reveals considerable swinging of that portion of the foot that includes the DELSEED region nearest the central γ axis, and is coupled to an appreciable relative twisting of the top and bottom of the nucleotide binding cleft in SUB. As an example, the 11.2Å distance of separation in SUB between lid atom Phe 424 CZ and Arg 189 CZ at the N terminal end of helix C, reduces to 10.4Å before increasing to 12.3Å during one cycle of oscillation, while the 16.5Å distance of separation between the same Phe 424 CZ and Glu 202 CD at the C terminal end of helix C, first increases to 18.0Å before reducing to 15.0Å during the same cycle of oscillation. This motion seems enabled by the torso's central β sheet as the twist angle between adjacent strands of the β sheet varies slightly as the head and foot domains rotate in opposite sense[40]. As before, this distortion of the nucleotide binding cleft is not seen in SUA.

We next examine the correlations of the computed motilities against the experimentally determined temperature factors before computing to what extent these three orthogonal modes reduce the RMSD between the closed and open β monomers. In the discussion, we will consider the sources of the variable stiffness characteristics in SUA and SUB.

D. Correlations with crystallographic temperature factors

We were interested to see how well the crystallographically determined Debye-Waller or B-factors for the three α chains as well as for the three β chains compared, in addition to their similarities to the computed motilities. The 3 α chains obtain all-atom RMSDs of around 0.7Å, and one might expect, barring crystal packing effects, very similar B plots. In fact, the crystallographic B-factors per C_α for chains A and C are quite similar (Figure 7A, solid lines), as expected, but chain B obtains a distinct signature (Figure 7B, solid line),

with 5 pronounced peaks in the head region, a reduced amplitude in the neck and shoulder region, and enhanced motility in the foot region. Superposed on these plots with dotted lines are the *unscaled* computed temperature factors of the first 50 modes (Figure 7B, dashed line) and of modes 2-50 (Figure 7A, dashed line). The experimental temperature signature of chain B is reproduced reasonably well by the contributions of the slowest 50 modes, with its distinct head peaks, helix C and DELSEED peaks as well as several other other torso and foot peaks accounted for. Intriguingly, the experimental temperature factors of chains A and C are best reproduced by excluding mode 1 in the sum, which similarly eliminates the distinct peaks in the head region. One interpretation of these data is that in the 2JDI crystal, chain B vibrates along all eigenmodes while chains A and C lack the slowest degree of freedom, perhaps due to their differing interaction with the central rotor proteins. The current computations consider only intra-monomer, not inter-monomer, packing interactions, and the possibility that the source of the variable experimental Debye Waller signatures for the three α chains might arise from variable symmetry axes activation is a novel concept for molecules as large as proteins. Laser spectroscopists have successfully activated single resonances (eigenfrequencies) in multi-atom systems in order to alter reaction rates[19,41]; perhaps the altered B chain Debye Waller factor profile in the crystal structure map is indicative of selective eigenmode damping.

The experimental temperature factors for chains D, E and F are shown in Figure 8. The two structurally similar subunits, D and F, display similar vibrational patterns indicated by the solid brown curve, while chain E obtains significantly higher B-factors for the C-terminal residues after the torso's final β strand, as well as an additional spike for those residues connecting the fist to the P-loop, as indicated by the dashed curve. Superposed on these curves in black are the computed B-factors due to the slowest 50 modes of chain F. The theoretical values reproduce some of the experimental features, obtaining similar head and foot motility profiles yet notably missing several peaks in the torso region. For example, the experimental peak at residues 238-242, a loop on the anterior surface of the torso's β sheet, is not predicted. As discussed, the computed motility profiles for chains D, E and F are almost indistinguishable, hence the source of the E chain's variable B signature is likely due to effects other than intra-minimum, equilibrium vibrations.

While experimental temperature factors include many effects other than the intra-monomer vibrations considered here, such as harmonic inter-monomer and crystalline

vibrations as well as anharmonic noise, nonetheless it might be instructive to determine whether these data support the central assertion of reduced motility at the posterior surface of the torso's β sheet in SUA compared to SUB. PDB-NMA predicts the C_α atoms in SUA and SUB to obtain average B-factors of $9.7\mathring{A}^2$ and $10.9\mathring{A}^2$. The C_α atoms posterior to the β sheet, α169-229 and β157-214, obtain average theoretical B-factors of $6.2\mathring{A}^2$ and $9.9\mathring{A}^2$, indicating the reduced mobility of this region in SUA compared to SUB. The average experimental C_α B-factors for SUA and SUB are $15.8\mathring{A}^2$ and $15.9\mathring{A}^2$. The average experimental B-factors for the C_α atoms posterior to the β sheet are $15.5\mathring{A}^2$ and $18.8\mathring{A}^2$, indicating once again that the posterior surface of the torso's β sheet obtains lower motility character in SUA than in SUB. In sum, the experimental B-factors do not contradict the predictions of NMA; support the observation that the nucleotide binding region experiences reduced motility; suggests the B-factor data of the α subunits to be more accurately modeled by NMA than those of the β subunits; and may indicate selective modal damping in an α subunit.

E. Interconversion of SUB structures with modes

By deforming the coordinates of SUB chain F along the directions of its three slowest modes, we tested to what extent those coordinates could reduce the RMSD between chains F and E (Figure 9). The initial RMSD of all mainchain heavy atoms of 3.8Å is reduced to 2.3Å using relative contributions of 25%, 45% and 30% of modes 1,2 and 3. The resultant structure shows that the transformation aligns the relative positions of the head, foot and torso domains but does not much improve the alignments within domains, that remain at 0.25Å, 1.2Å and 0.53Å RMSD from those of chain E. For example, alignment of the crystal F and E chains shows a distance of separation of their C termini of 8.5Å that reduces to 1.5Å for the normal-mode-deformed F chain. Likewise, the N termini in the crystal coordinates are 4.5Å apart, which reduces to 2.4Å for the NM-deformed chain. Within the torso domain, however, only slight improvements to the RMSD are achieved, with observed realignment of the nucleotide binding cleft not modeled as well by the slowest three modes. The cleft separation, for example, from C helix C_α 203 to mobile lid C_α 420 in chain F is 13.8Å and in chain E is 5.1Å. The NM-deformed F chain reduces this to 11.1Å.

A similar analysis of chain D reduces an initial RMSD to chain E of 3.8Å to 3.6Å with use

of 8.5 kT of mode 1, to 2.9Å with 17.3 kT of mode 2, and to 2.7Å with 8.5 kT of mode 3. The importance of natural or innate flexibility in effecting the open to closed transformation of β subunits was noted by Böckmann and Grubmüller, based on MD simulations of unliganded, open β subunits. They found fast, spontaneous and nucleotide-independent closure of the open β subunit, with changes not localized to the nucleotide binding region and not exerted from adjacent α subunits: "the main driving force for the closure is internal to the β-subunit" they concluded[38].

III. DISCUSSION

A. Design and Flexibility of Subunits

SUA and SUB present very similar topologies and folds leading to similar flexibility profiles. A long linker arm straddles a central torso domain to interconnect similar head and foot domains. A seven stranded parallel β sheet spans the torso from the ventral surface near the head to the dorsal surface near the foot, and divides the torso into an anterior region involved with inter-subunit packing and a posterior region that includes the nucleotide binding cleft. Both have an important short α helix at the end of the linker arm embedded tightly in the foot domain. This helix forms nonbonded interactions with residues forming the torso's eighth, antiparallel β strand (in SUB the pattern of inter-strand hydrogen bonding precludes its designation as a β strand); the N terminal end of the long α helix after the arginine finger; the C terminal end of the foot's third α helix and the N terminal end of its fourth α helix whose connecting loop constitutes the mobile lid or the strut; as well as with the C terminal end of the torso's helix B. The fist, in other words, while still near the N terminal end of the polypeptide chain (residues 138-143), also coordinates the motion of foot residues, including the critical lid or strut, as well as torso residues. Specifically, as indicated in Figure 6C and D, these regions, like the fist residues, obtain very small motilities, indicating the critical importance of the fist in coordinating the motions while maintaining the structural integrity of the chain's fold.

This design leads to similar motility profiles, with the softest motilities associated with a side-wise rolling, a flexing towards the central axis, and a twisting about the central axis of the head and foot domains. While the inter-domain motions of the head, foot and

torso appear largely similar between SUA and SUB, important differences exist between the motility profiles of the region posterior to the torso's β sheet: the nucleotide binding region. In SUB the nucleotide binding cleft exhibits pronounced opening and closing motions, motilities absent in SUA, and points to an unsurprising difference between enzymes and structural proteins. Enzymes require entry and exit of reactants and products in a manner that predicates reaction rates, whereas structural proteins have no need of such intra-domain motilities. What design features allow one chain to be an active enzyme, the other not?

B. Source of Variable Torso Stiffness

In SUA the residues forming the foot domain move in lockstep with the fist residues and also with all the residues comprising the posterior surface of the torso's β sheet. In SUB the residues forming the foot and fist move together with only helix B of the posterior surface: helix C moves *en masse* with the shoulder and residues of the anterior surface. Why? Certainly the presence in SUA of the foot's strut element and the resultant tight packing between strut residue αTyr 433 and helix C residue αArg 219 creates a significant obstruction to intra-cleft motilities. But in addition to this localized distinction, distributed differences exist between SUA and SUB in terms of the distribution of NBI. The 35 arm residues (α Asp 116 - Ile 150 and β Asp 103 - 137) for example, pack more tightly in SUA, with 1186 NBI between arm atoms and non-arm atoms, and 789 such NBI in SUB. Also, as pointed out in the Results section, the diagonal distance across the torso as measured by the distance of separation of the C_α atoms of the first and last arm residues is 33Å in SUB and 28Å in SUA, another indication of a more compact torso arrangement in SUA. The less tightly packed arm segment of SUB obtains two additional elements of secondary structure: a 310 helix (Phe 123 - Glu 125), as well as a short antiparallel β sheet preceding the fist (Ile 132 - Leu 133 and Tyr 146 - Ala 147), both absent in SUA.

Another element that seems critical to the distinct motility profiles centers on the interface of the foot and torso domains and pertains to the fold of the chain immediately after α Arg 373 and β Arg 356. This so-called arginine finger is equivalently situated in SUA and SUB: contributed by the foot domain but oriented towards the anterior surface of the β sheet, at the dorsal surface between the torso and the arm. In SUA the chain after Arg 373 turns away from the dorsal interface and inserts into the cleft formed at the junction of the arm

and fist where the two β strands preceding the fist meet. Likely this is the reason that SUA cannot form a β structure here: any potential β strand contributed by the arm segment is displaced by this loop after the arginine finger. This tight packing in SUA effectively creates a block structure where fist and foot motility transfers *en masse* to helix B and, due to the strut, to helix C. In SUB the residues after Arg 356, instead of folding away from the dorsal surface, fold towards it, creating the space that allows the formation of the locally stiff antiparallel β strand that precedes the fist. This arrangement eliminates the tight packed, block-like structure and creates the possibility of intra-domain motion, with helix B moving with the foot domain, and helix C moving as part of the shoulder and anterior surface of the torso.

The eigenmodes of SUA and SUB, therefore, demonstrate the two qualities that play off each other so that two chains with identical folds have different motilities: spaciousness provided by regions with relatively low density of NBI against local stiffness elements, such aditional elements of secondary structure. Lack of tight packing in SUB is supplemented not only by the presence of additional rigid elements of secondary structure, but also by inclusion of additional prolines. SUB has 23 while SUA has 17 of them. Rigid body motion seems enabled by distributed, high density of NBI forcing such regions to move *en masse*. Relative motion within a domain or region requires sufficient space to enable the various elements to move in an opposing sense. Such spaciousness likely could result in localized fraying or unfolding of the polypeptide chain, were it not offset by these elements of local stiffness. In both cases there is effective and fine-tuned transmission of stiffness throughout the chain. The distributed nature of the "control" of mobility characteristics minimizes likelihood of disruption but also permits higher precision. For example, the absence of the strut element in SUB permits motility within the nucleotide binding cleft, but this additional degree of freedom is not disorderly or haphazard: many nonlocalized, distributed elements conspire to control the expression of this degree of freedom.

C. Intra-monomer oscillations within assembly

Eigenmodes were computed for isolated α and β chains without regard to the additional inter-monomer NBIs in the assembly, hence steric clashes were expected when these intra-monomer modes were activated within the assembly. Unexpectedly, steric inter-monomer

clashes are avoided in the assembly when the isolated-monomer modes were activated simultaneously. The interfaces maintain their interdigitation during activation of each (intra-monomer) mode, with the projections of one subunit maintaining closely similar dispositions with the concavities of its neighbor. This effect seems to be caused by the relative immobility of those residues involved with inter-monomer interactions.

In particular, a ring of connectivity that extends around the assembly at the level of the superior surface of the torso maintains close interdigitations, with shoulder elements of one subunit packing with arm elements of the neighboring subunit. Specifically, at the dorsal surface of SUA, arm residues α Pro 134 - Pro 138 form a loop construct that latch tightly with the neighbor's shoulder loop β Pro 101 - Pro 107, with α Ile 136 - Ile 137 buttressed between the neighbor's shoulder loop and the N terminal (inner) end of its helix C. Both interdigitating loops at this dorsal surface are braced by proline residues that provide the requisite rigidity to these latch elements.

At the ventral surface of SUA, meanwhile, shoulder loop residues α Ala 114 - Pro 120 form the loop construct that together with helix C latch onto the neighbor's β Pro 121 - Glu 125 arm residues, with the protrusion of β Phe 123 maintaining a tightly coordinated orientation with the neighboring subunit during thermal activation. Note that one of the two bracing prolines in the SUB's arm loop is replaced by a short 310 helix at residues β Phe 123 - Glu 125 that seems to confer the requisite rigidity to help maintain hexamer integrity.

Activating the oscillatory motion of each mode simultaneously therefore suggests a relatively immobile anterior torso surface coordinating hexamer stability while the foot and posterior torso surface seem "free" to oscillate independently of its neighbors. This feature, of isolated, individual components comprising an assembly already possessing the flexibility characteristics suitable for the ensemble and not imposed by the assembly are surprising and indicative of an active two-way selection pressure from the ground up as well as from the top down[42]. Initial assumptions, that the rotary catalysis mechanism of ATP synthase is governed by the rotation of the central $\gamma\delta\epsilon$ unit that forces each SUB into different conformations, ignores these intrinsic propensities that help explain the observation of rotary catalysisF in rotorless hexamers.

IV. CONCLUSION

We examined the reasons why two proteins with nearly identical topology and fold but with different primary sequences behave very differently within the same assembly: one as a structural protein the other as an enzyme. Without distorting the PDB coordinates, we computed the distinct symmetry axes of each protein via PDB-NMA and discovered unique signatures that help explain their differing behaviors. PDB-NMA consistently demonstrates the intrinsic flexibility around active sites in enzymes where reactants and reaction products enter and exit. Structural proteins like SUA do not develop the flexibility characteristics associated with interdomain motilities, where similarly disposed regions move, more simply, with block-like character. Active site motility is enabled by relatively low NBI or packing densities in critical junctures that create sufficient space to permit opening and closing movements. Any resultant structural weakness is offset by local stiffness elements, including β sheets, helices and prolines.

In addition to developing insights into the particular three-dimensional architecture of a stably folded protein, PDB-NMA demonstrates how locally stiff regions may obtain very high temperature factors. Residues with high experimental Debye-Waller factors likely are not disordered, but orderedly mobile, an observation supported not only by crystallographic data but also by MD simulations that observe similar long term behavior as NMA. Enzymes function as machines that are firm and flexible, and with flexibility characteristics that are reliable and reproducible.

We deformed the coordinates of a closed β chain along the directions of its slowest three modes to achieve better overlap with the coordinates of the open chain. An initial RMSD of 4Å between these structures was thereby reduced to 2Å, without creating steric clashes. The resultant structure achieves close inter-domain fits of the head, foot and torso and less close fits for intra-domain shifts, especially of the nucleotide binding region. During the structural transformation of the β subunit this region undergoes major shifts in solvation, a feature not modeled by the current analysis and likely a major reason for the poorer fit. Finally, PDB-NMA permits examination of observed and computed temperature factors to search for clues in mobility profiles of different chains. In the case of the three α subunits in 2JDI, two distinct B-factor profiles were observed that might be indicative of modal suppression of the slowest mode in these two chains.

ACKNOWLEDGMENTS

I thank Prof. García-Hernández for providing data of the MD simulation of the liganded and unliganded β subunits of PDB entry 2JDI and Daniel Ben-Avraham for many helpful discussions. This work is supported in part by the M. Hildred Blewett Fellowship of the American Physical Society, www.aps.org.

REFERENCES

[1]T. Xu, V. Pagadala, and D. M. Mueller, "Understanding structure, function, and mutation in the mitochondrial ATP synthase," Microbial Cell **2**, 105–125 (2015).

[2]J. E. Walker, "The ATP synthase: the understood, the uncertain and the unknown," Biochemical Society Transactions **41**, 1–16 (2013).

[3]A. E. Senior and S. Nadanaciva, "The molecular mechanism of ATP synthesis by F_1F_o-ATP synthase," Biochimica et Biophysica Acta **1553**, 188–211 (2002).

[4]W. Junge and N. Nelson, "ATP synthase," Ann. Rev. Biochem. **84**, 631–57 (2015).

[5]M. Yoshida, E. Muneyuki, and T. Hisabori, "ATP synthase – a marvelous rotary engine of the cell," Nature Rev Mol Cell Biol **2**, 669–77 (2001).

[6]S. B. Needleman and C. D. Wunsch, "A general method applicable to the search for similarities in the amino acid sequence of two proteins," J. Mol. Biol. **48**, 443–53 (1970).

[7]P. D. Boyer, "A perspective of the binding change mechanism for ATP synthesis," FASEB J. **3**, 2164–78 (1989).

[8]J. Pagan and A. E. Senior, "Tight ATP and ADP binding in the noncatalytic sites of Escherichia coli F_1-ATPase is not affected by mutation of bulky residues in the 'glycine-rich loop'," FEBS Lett. **273**, 147–9 (1990).

[9]A. N. Malyan, "Noncatalytic nucleotide binding sites: Properties and mechanism of involvement in ATP synthase activity regulation," Biochemistry **78**, 1512–23 (2013).

[10]P. D. Boyer, "A research journey with ATP synthase," J. Biol. Chem. **277**, 39045–61 (2002).

[11]K. Miwa and M. Yoshida, "The alpha 3 beta 3 complex, the catalytic core of F_1-ATPase," PNAS **86**, 6484–7 (1989).

[12]T. Uchihashi, R. Iino, T. Ando, and H. Noji, "High-speed atomic force microscopy reveals rotary catalysis of rotorless F_1-ATPase," Science **333**, 755–8 (2011).

[13]W. Junge and D. J. Müller, "Seeing a molecular motor at work," Science **333**, 704–5 (2011).

[14]J. B. Marion, *Classical Dynamics of Particles and Systems* (Academic Press, NY, 1970).

[15]H. Na, D. ben-Avraham, and G. Song, "Universality of vibrational spectra of globular proteins," Phys. Biol. **13**, 016008 (2016).

[16]D. ben-Avraham, "Vibrational normal-mode spectrum of globular proteins," Phys. Rev. B **47**, 14559 (1993).

[17]R. Elber and M. Karplus, "Low-frequency modes in proteins: Use of the effective-medium approximation to interpret the fractal dimension observed in electron-spin relaxation measurements," Phys. Rev. Lett. **56**, 394 (1986).

[18]A. Cooper, "Thermodynamic fluctuations in protein molecules," Proc. Nat. Acad. USA **73**, 2740–1 (1976).

[19]R. Hoffmann, "Exquisite control," American Scientist **88** (2000), 10.1511/2000.1.14.

[20]Y.-H. Sanejouand, "Functional information from slow mode shapes," in *Normal Mode Analysis: Theory and Applications to Biological and Chemical Systems*, edited by Q. Cui and I. Bahar (Chapman and Hall, 2005).

[21]A. Pentland and S. Sclaroff, "Modal matching for correspondence and recognition," IEEE Trans on Pattern Analysis and Machine Intelligence **17**, 545–61 (1997).

[22]M. Levitt, C. Sander, and P. S. Stern, "The normal modes of a protein: Native bovine pancreatic trypsin inhibitor," Int. J. Quantum Chem. **24**, 181–99 (1983).

[23]D. Ringe and G. A. Petsko, "Mapping protein dynamics by X-ray diffraction," Progress in Biophysics and Molecular Biology **45**, 197–235 (1985).

[24]M. M. Tirion, "Large amplitude elastic motions in proteins from a single-parameter, atomic analysis," Phys. Rev. Lett. **77**, 1905 (1996).

[25]H. Na and G. Song, "The performance of fine-grained and coarse-grained elastic network models and its dependence on various factors: Performance of fine and coarse-grained ENM," Proteins Structure Function and Bioinformatics **83** (2015), 10.1002/prot.24819.

[26]M. M. Tirion and D. ben-Avraham, "Atomic torsional modal analysis for high-resolution proteins," Phys. Rev. E **91**, 032712 (2015).

[27]M. M. Tirion, "On the sensitivity of protein data bank normal mode analysis: An application to GH10 xylanases," Phys. Biol. **12**, 066013 (2015).

[28]M. Levitt, "Molecular dynamics of native protein. I. Computer simulation of trajectories," J. Mol. Biol. **168**, 595–620 (1983).

[29]M. Levitt, M. Hirshberg, R. Sharon, and V. Daggett, "Potential energy function and parameters for simulations of the molecular dynamics of proteins and nucleic acids in solution," Comp. Phys. Communication **91**, 215–31 (1995).

[30]H. M. Berman, J. Westbrook, Z. Feng, G. Gilliland, T. N. Bhat, H. Weissig, I. N. Shindyalov, and P. E. Bourne, "The protein data bank," Nucleic acids research **28**, 235–242 (2000).

[31]J. P. Abrahams, A. G. Leslie, R. Lutter, and J. E. Walker, "Structure at 2.8 å resolution of F_1-ATPase from bovine heart mitochondria," Nature **370**, 621–8 (1994).

[32]Q. Cui, G. Li, J. Ma, and M. Karplus, "A normal mode analysis of structural plasticity in the biomolecular motor F_1-ATPase," J. Mol. Biol. **340**, 345–72 (2004).

[33]W. Zheng, "Normal-mode-based modeling of allosteric couplings that underlie cyclic conformational transition in F_1 ATPase," Proteins **76**, 747–62 (2009).

[34]M. W. Bowler, M. G. Montgomery, A. G. W. Leslie, and J. E. Walker, "Ground state structure of F_1-ATPase from bovine heart mitochondria at 1.9A resolution," J. Biol. Chem. **282**, 14238–42 (2007).

[35]D. Ringe and G. A. Petsko, "'The glass transition' in protein dynamics: What it is, why it occurs, and how to exploit it," Biophys. Chem. **105**, 667–80 (2003).

[36]M. M. Tirion and D. ben-Avraham, "Normal mode analysis of g-actin," J. Mol. Biol. **230**, 186195 (1993).

[37]O. Hahn-Herrera, G. Salcedo, X. Barril, and E. García-Hernádez, "Inherent conformational flexibility of F_1-ATPase α subunit," Biochim. Biophys. Acta **1857**, 1392–402 (2016).

[38]R. A. Böckmann and H. Grubmüller, "Conformational dynamics of the F_1-ATPase β-subunit: A molecular dynamics study," Biophys. J. **85**, 1482–91 (2003).

[39]S. Hayward, A. Kitao, and N. Gō, "Harmonic and anharmonic aspects in the dynamics of BPTI: A normal mode analysis and principal component analysis," Protein Sci. **3**, 936–43 (1994).

[40]R. B. Fenwick, L. Orellana, S. Esteban-Martin, M. Orozco, and X. Salvatella, "Correlated motions are a fundamental property of β-sheets," Nature Communications **5** (2014),

10.1038/ncomms5070.

[41]S. A. Kandel and R. N. Zare, "Reaction dynamics of atomic chlorine and methane: Importance of methane bending and torsional excitation in controlling reactivity," J. Chem. Phys. **109**, 9719–27 (1994).

[42]R. Iino and H. Noji, "Rotary catalysis of the stator ring of F_1-ATPase," Biochim. Biophys. Acta **1817**, 1732–39 (2012).

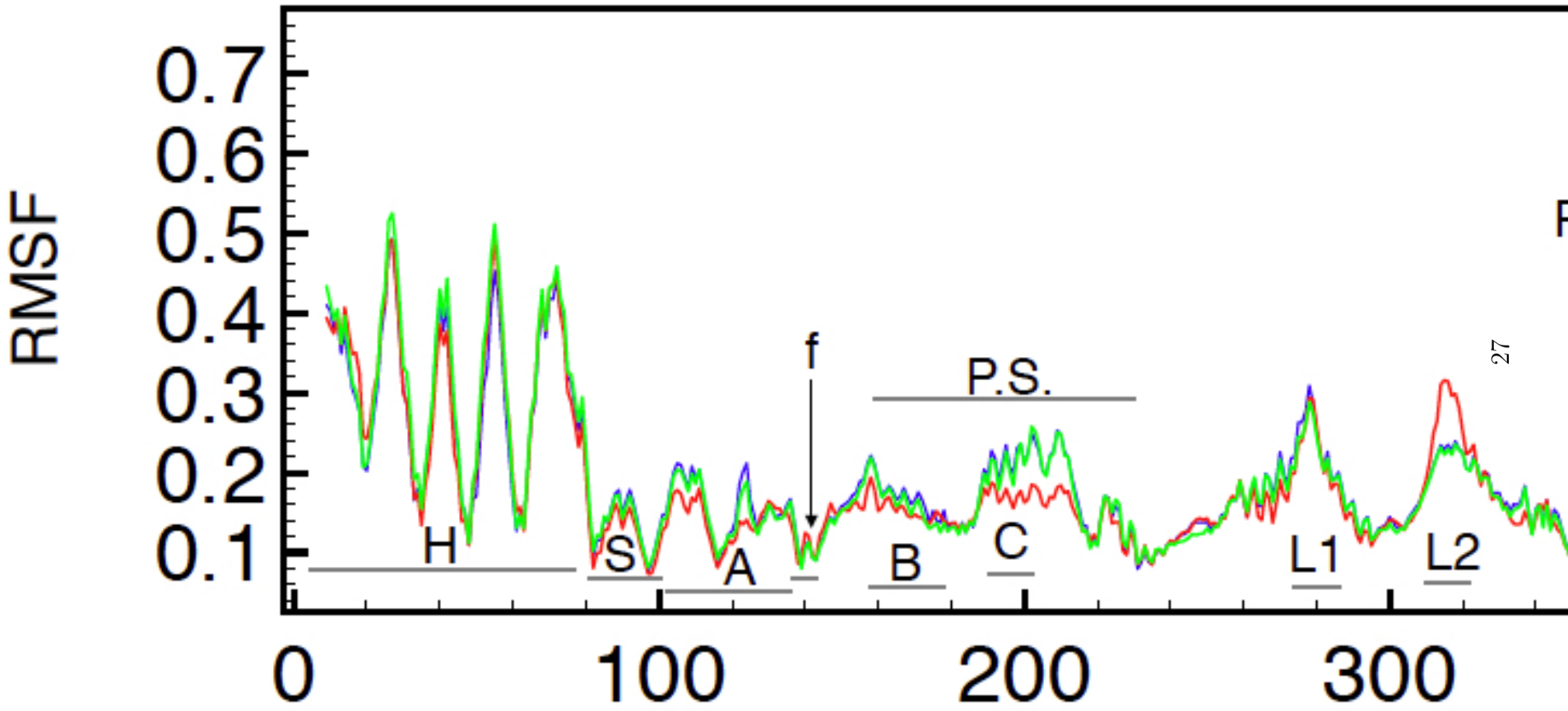
RMSF
0.7
0.6
0.5
0.4
0.3
0.2
0.1
0
100
200
300
H
S
A
f
B
C
P.S.
L1
L2

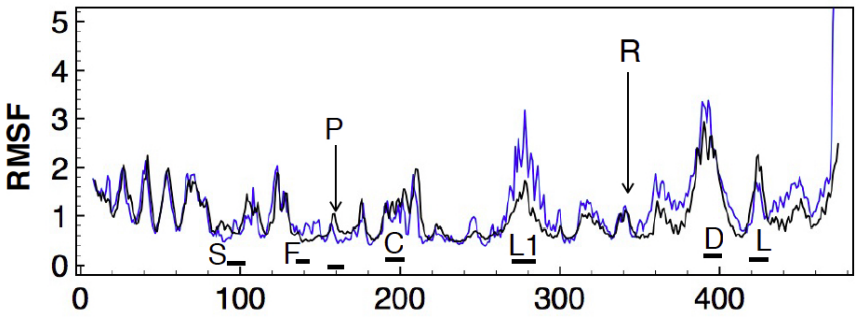

FIG. 4. The RMSF in Å per C_α obtained from a 100ns MD simulation of hydrated, isolated and liganded subunit β (chain F) in blue[37] and of the same chain, unliganded, computed from the slowest 50 normal modes in black. The close overlap indicates that the long term motility of the polypeptide chain is well captured by the harmonic analysis, with only slight mismatches in the magnitude of peaks associated with the fist region and P-loop region, likely due to the absence of nucleotide in the PDB-NMA; a different magnitude for the L1 peak near the γ rotor axis; and some mismatch in magnitude in the region immediately after the arginine finger and after the mobile lid region. Both the DELSEED loop as well as the mobile lid region in the foot domain overlap closely.

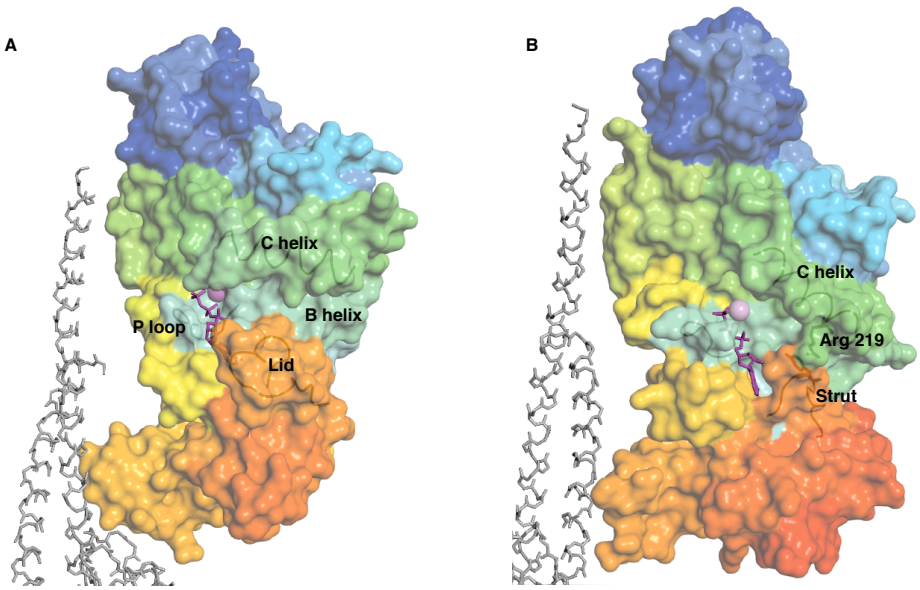

FIG. 5. Surface representations of the ventral surfaces of SUB (left) and SUA (right) showing the nucleotide binding clefts with ATP colored magenta and Mg as a pink sphere. The N and C terminal domains of subunit γ's are shown in a gray stick representation. SUA and SUB are colored with a rainbow scheme with the N terminal, head domain in dark blue, the shoulder and fist (visible beneath the strut in B) in cyan and the C terminal foot domains orange and red. The P-loop, to the left of ATP, extends as helix B in light blue and forms the base of the nucleotide binding cleft. The top of this cleft is formed by helix C and the bottom of the cleft by the mobile lid (A) or the rigid strut (B). In SUB helix C and the lid experience pronounced swinging motions in eigenmodes 1, 2 and 3, motions absent in SUA where strut residue Tyr 433 forms extensive steric interactions with helix C residue Arg 219. Figures prepared in PyMol.

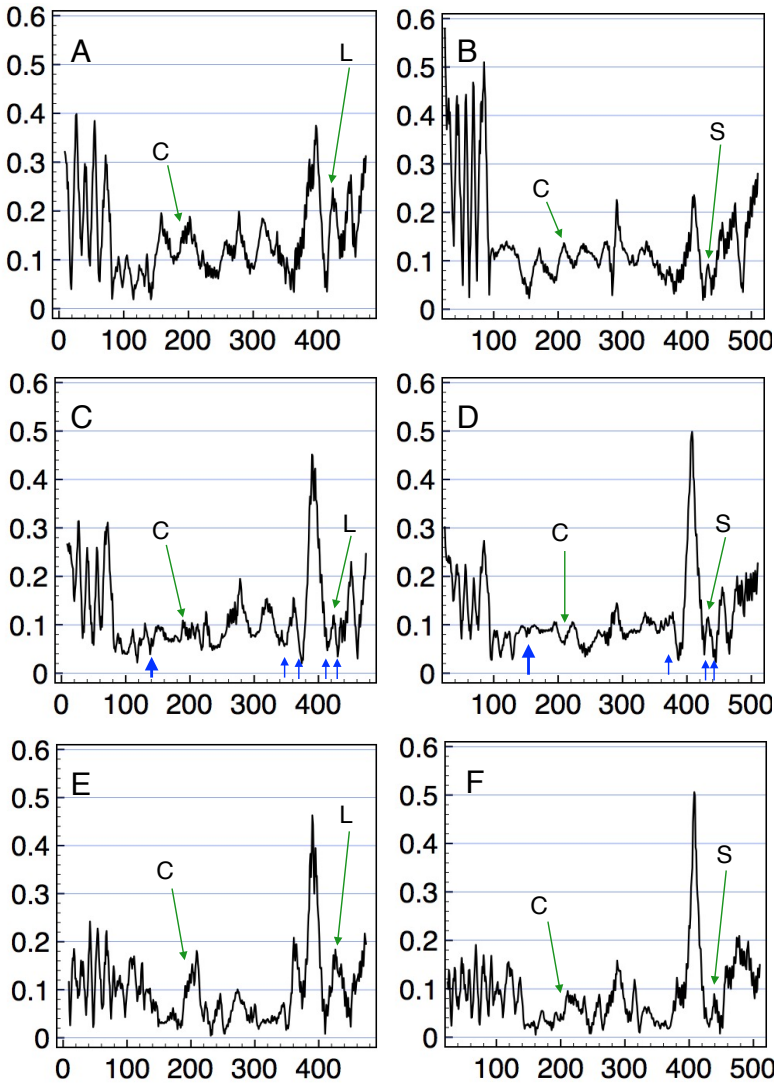

FIG. 6. RMSF in Å per C_α for mode 1 (A and B), mode 2 (C and D) and mode 3 (E and F) with left images for SUB and right images for SUA. Peaks associated with helix C and either the lid L (SUB) or the strut S (SUA) are indicated by slanted green arrows. The short vertical blue arrows indicate regions of low motility near to the fist residues. and demonstrate greater motility in SUB than SUA. Mode 1, a sidewise rolling of the head and foot domains about an axis roughly aligned with helix B, exhibits reduced head motility and greater foot motility in SUB compared to SUA. The increased motility at the posterior surface of the torso's β sheet appears as a chewing type motion across the nucleotide binding cleft. Mode 2 is a flexing towards and away from the central axis of the head and foot domains about an axis aligned with the fist helix with the torso relatively immobile. That portion of the nucleotide binding cleft furthest removed from the fist-helix, namely the N terminal end of helix C, experiences a small spike in SUB not present in SUA and again pertains to the greater binding cleft motility seen in this subunit. Mode 3 presents as a twist type motion of the head and foot domains where, like mode 1, the helix C peak and the lid/strut peak

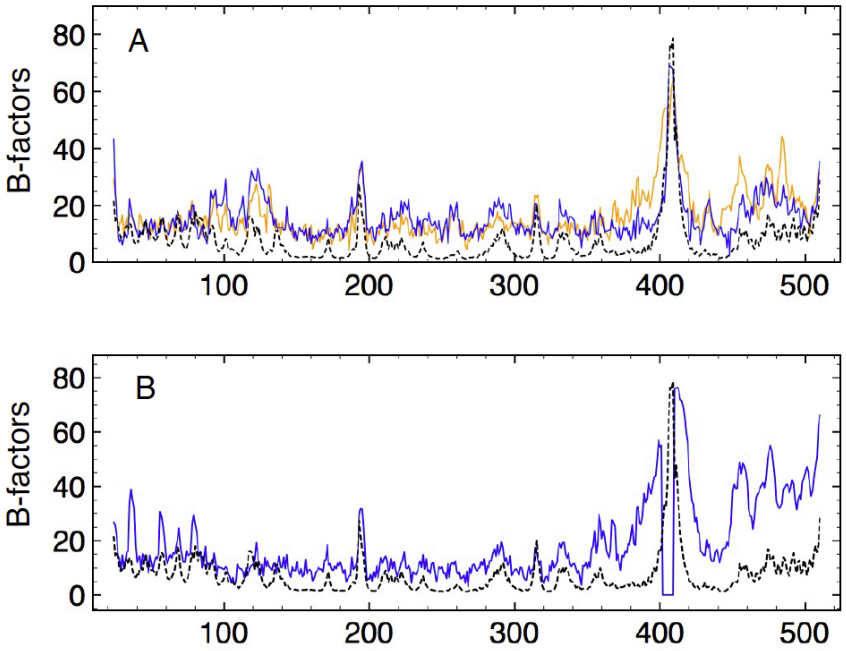

FIG. 7. Crystallographic B-factor in Å^2 per C_α for the three α subunits: chains A and C in orange and blue in top panel and chain B in blue, bottom panel. The PDB entry for chain B misses residues 402-409. Superposed in broken black line, the unscaled computed B-factors derived from the sum of modes 2-50, top panel, or 1-50, bottom panel. The experimental B-factor plot for chain B with the distinct head peaks is better reproduced by excluding mode 1 in the sum.

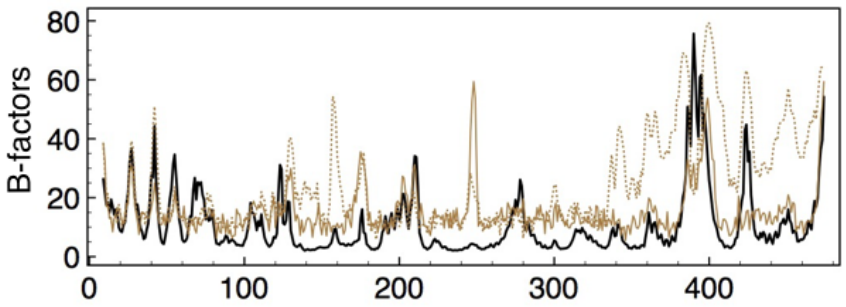

FIG. 8. Crystallographic B-factors in $Å^2$ per C_α for the β subunits: chains D and F obtain similar B-factor profiles shown by solid brown curve and chain E with dashed brown curve. The unscaled theoretical values are superposed in solid black. Unlike the D and F chains whose experimental B-factors are reasonably well modeled by PDB-NMA, the distinct experimental B-factor curve of chain E is less well modeled. Each crystalline hexamer unit obtains one unliganded, β subunit with altered solvation characteristics due to its open configuration. Reduced statistics combined with possible greater variability in conformation of foot domain, including the fist, might explain the mismatch. The peak at 245 corresponds to a loop on the anterior surface of the torso's β sheet, at high radius, and is involved perhaps with inter-hexamer packing interactions. The enhanced P-loop peak (156-163) motility is likely due to the absence of nucleotide and cation.

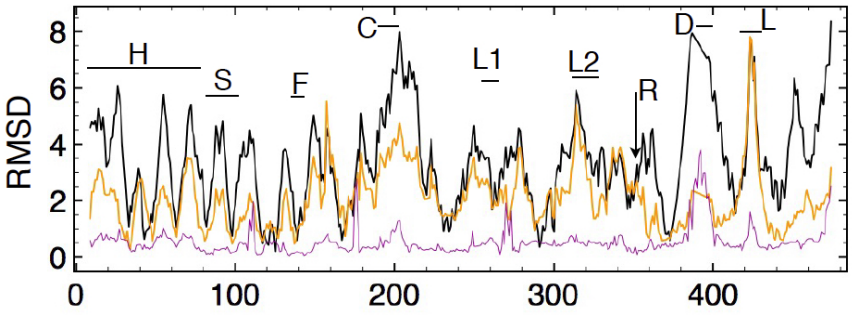

FIG. 9. RMSD in Å per C_α between the PDB coordinates of chain E (open conformation) and chain F (closed conformation) in black, with an overall RMSD of 3.8Å. Horizontal bars identify regions as defined in Figure 3. A similar curve for the RMSD between chain E and the normal mode deformed chain F, shown in orange, obtains an overall RMSD of 2.3Å. For comparison, the RMSD curve for the similarly shaped closed chains D and F, with an overall RMSD of 0.6Å, is shown in purple. These data show that the initial large mismatch in the alignment of the head, shoulder and arm residues as well as the foot residues after the arginine finger, improves significantly after adjusting chain F coordinates along the slowest three modes. The fit of the lid (L) region does not improve, suggesting a nonharmonic contribution to the shift of this region during the interconversion of the open and closed conformations. For the torso, there is improvement in the fit in that region on the posterior surface that includes the helix C residues. The fit of the remainder of the torso region is not much improved, indicating that shifts within this region are also less well modeled by harmonic, intra-minimum oscillations exclusively. PDB 2JDI chain E lacks residues 388-395 within the DELSEED region.